Aust. J. Phys., 1982, **35**, 475–99

A New Class of Atomic States: The 'Wannier-ridge' Resonances

F. H. Read

Department of Physics, Schuster Laboratory,
The University, Manchester M13 9PL, England.

Abstract

The evidence for the existence of systems that are dominated by electron–electron correlations is briefly reviewed, with particular attention being paid to (i) the processes of near-threshold electron-impact ionization and excitation of atoms and (ii) the structure of atomic doubly excited states and Feshbach resonances. New evidence is then presented for the existence of atomic resonances in which two excited electrons both have high values of the principal quantum number n (up to $n = 8$), and in which these two electrons reside on or near the Wannier ridge (i.e. with $\boldsymbol{r}_1 \approx -\boldsymbol{r}_2$).

1. Introduction

The independent-electron model is usually an excellent first approximation when considering atomic structure or electron–atom collision processes, and it can be improved perturbatively to take account of the effects of electron–electron correlations. Nevertheless there remain some essentially non-perturbative systems in which these correlations are of major importance and for which the electrons cease to move approximately independently of each other. These *correlation-dominated* examples include atomic states in which electron–electron correlations are so strong that the independent-electron model fails to provide an adequate starting basis for classification purposes (see e.g. Fano 1976; Herrick and Kellman 1980).

In the present paper we start in Section 2 with a brief review of the evidence for the dominance of electron–electron correlations in certain electron–atom collision processes, in particular the processes of near-threshold electron-impact ionization and excitation of atoms. In Section 3 the problem of the classification of correlation-dominated atomic states is discussed: examples of the experimental evidence are presented and the relevant theoretical models are briefly described. In Section 4 experimental results are given of the observation of atomic resonance states of a new class. In these states two excited electrons both have high values of the principal quantum number n. The dominance of electron–electron correlations in these states is discussed, and a simple model is described which indicates that in at least some of these resonances the two electrons reside on or near the Wannier ridge (i.e. with $\boldsymbol{r}_1 \approx -\boldsymbol{r}_2$). A feature that the systems discussed in Sections 2, 3 and 4 have in common is that two electrons both reside at large distances ($\gtrsim 10$ Å) from a positive ion core, and that the sum of their kinetic energies is less than about 0·5 eV.

2. Correlations in Threshold Ionization and Excitation Processes

(*a*) *Threshold Ionization*

The archetypal threshold process showing evidence of long-range electron–electron correlations is that of near-threshold ionization of an atom by electron impact:

$$e+A \rightarrow A^{+}+e+e. \tag{1}$$

We start with this because it embodies in a simple way some important features that are present also in other two-electron correlated systems. The energy E above threshold, which is also equal to the total free (i.e. non-internal) energy of the three charged particles in the final state, is assumed to be very small (much less than the Rydberg energy R). The low value of E causes correlation effects to play a dominant role, thus allowing them to be observed. The same correlation effects are seen also in photo-double-detachment (Bryant *et al.* 1981).

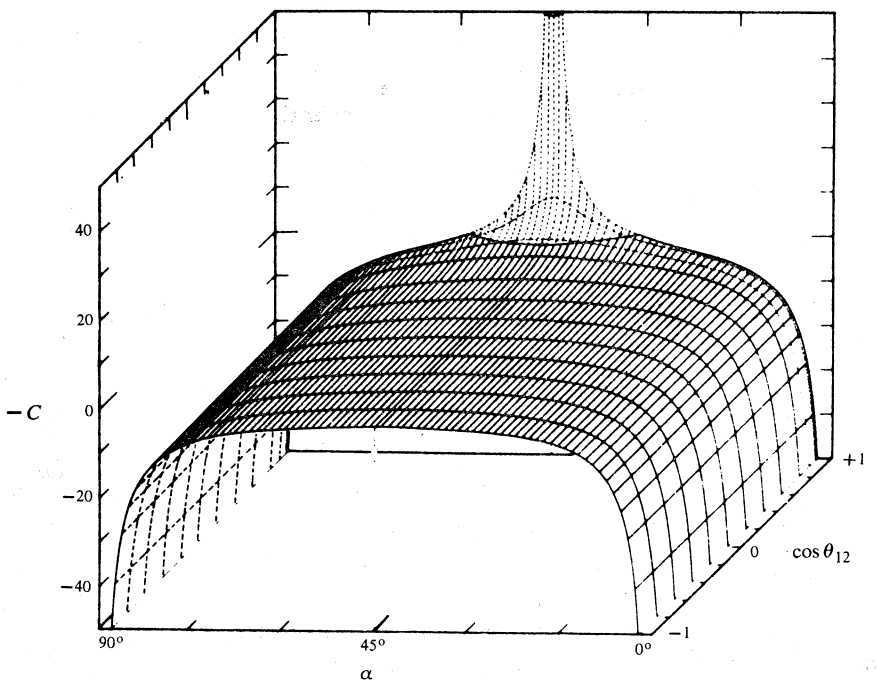

Fig. 1. Relief plot of $-C(\alpha, \theta_{12})$ with $R = 1$ and $Z = 1$. [Lin 1974; Fano and Lin 1975.]

The essential physics of the threshold-ionization process can be understood by working in terms of the hyperspherical coordinates

$$R = (r_1^2+r_2^2)^{\frac{1}{2}}, \qquad \alpha = \arctan(r_2/r_1), \qquad \theta_{12} = \arccos(\boldsymbol{r}_1 . \boldsymbol{r}_2), \tag{2}$$

where $\boldsymbol{r}_1$ and $\boldsymbol{r}_2$ are the positions of the two electrons with respect to the positive ion (taken to be a point particle for the present argument). These coordinates define the shape and size of the triangle that has the three charged particles as vertices.

Three further coordinates correspond to Euler angles defining the orientation of the triangle in the laboratory system, but because of the low value of E the system is essentially isotropic in these angles, which therefore need not be considered further.

In terms of the hyperspherical coordinates, the potential energy of the system of two electrons and a positive ion of charge Ze is (in a.u.)

$$V = -C(\alpha, \theta_{12})/2R, \tag{3}$$

where

$$C(\alpha, \theta_{12}) = \frac{2Z}{\cos\alpha} + \frac{2Z}{\sin\alpha} - \frac{2}{(1-\sin 2\alpha \cos\theta_{12})^{\frac{1}{2}}}. \tag{4}$$

Fig. 1 shows $-C$ as a function of α and $\cos\theta_{12}$ (over the range $\theta_{12} = 0$ to π only), for $Z = 1$. We see a spike (at $\alpha = \frac{1}{4}\pi$, $\theta_{12} = 0$) corresponding to electron–electron repulsion, and two valleys (at $\alpha = 0$ and $\frac{1}{2}\pi$) corresponding to electron–ion attraction. In the vicinity of the point $\alpha = \frac{1}{4}\pi$, $\theta_{12} = \pi$, which is often referred to as the *Wannier point*, we see that a saddle-shaped region exists, since $-C$ decreases as α diverges from $\frac{1}{4}\pi$ but increases as θ_{12} diverges from π. Note that the saddle region is shallow, and that the potential therefore varies little over rather wide ranges of values of α and θ_{12}. At the Wannier point itself we have $\boldsymbol{r}_1 = -\boldsymbol{r}_2$, so that the two electrons are at equal distances from, and on opposite sides of, the positive ion. As we shall see later, the saddle region plays a crucial role in determining the behaviour of a variety of systems containing two slow electrons.

The dependence of V on α and θ_{12} in the region of the Wannier point is

$$V_W = (2\sqrt{2}/R)\{-(Z-\tfrac{1}{4}) + \tfrac{1}{32}(\theta_{12}-\pi)^2 - \tfrac{1}{8}(12Z-1)(\alpha-\tfrac{1}{4}\pi)^2 + \ldots\}. \tag{5}$$

We see that the effective nuclear charge is $Z-\frac{1}{4}$, a point to which we shall return later. We see also that the dependence on θ_{12} is that of an attractive simple harmonic potential, giving a form of stability to the θ_{12} motion and causing the two electrons to tend to move to opposite sides of the positive ion. In contrast to this, the dependence on α gives rise to an instability in the neighbourhood of the Wannier point. The potential energy is a maximum at $\alpha = \frac{1}{4}\pi$ (for given values of R and θ_{12}), and so the system tends to move away from this value of α, causing the ratio r_1/r_2 to diverge from unity. This has been called the radial correlation instability (Rau 1971). The region of potential mapped out near the Wannier point as R is varied (i.e. the region for which $\boldsymbol{r}_1 \approx -\boldsymbol{r}_2$) is called the *Wannier ridge* (see e.g. Fano 1980).

(*b*) *Wannier Theory*

The way in which the potential energy (5) determines the behaviour of the three-particle system at low values of the excess energy E was first made clear by Wannier (1953), who integrated the classical equations of motion for this potential energy. To see why the classical treatment is justified it is useful to consider the critical radius

$$R_c = C(\tfrac{1}{4}\pi, \pi)/2E = (4Z-1)/E\sqrt{2}, \tag{6}$$

at which $|V| = E$. Ionization occurs when the system starts with $\alpha \approx \frac{1}{4}\pi$ and then develops in such a way that as R increases α stays in the vicinity of $\frac{1}{4}\pi$ until R becomes greater than about R_c. In this way the system keeps away from the negative potential energy region of the valleys, so that $|V|$ is subsequently able to continue to decrease,

with the result that the two electrons both eventually become free. If on the other hand R_c is reached when the system is far from the Wannier ridge then the attraction of the valleys will dominate so that $|V|$ cannot subsequently decrease to zero, with the result that one of the electrons becomes bound to the positive ion and only one electron is left free to escape. The probability distribution in α at $R = R_c$ therefore determines the relative probabilities of double escape (i.e. ionization) and single escape (i.e. excitation). The initial value of θ_{12} is less critical, since as R increases θ_{12} tends to converge to π, either by a damped oscillatory motion or monotonically. Each electron has of course a wavelength λ, and the magnitude of this increases as E decreases, but the ratio of λ (at the Wannier point and at $R = R_c$) to R_c decreases with E:

$$\lambda(R=R_c, \alpha=\tfrac{1}{4}\pi, \theta=\pi)/R_c = 2\pi E^{\frac{1}{2}}/(4Z-1). \tag{7}$$

We see therefore that at sufficiently low values of E the electrons can be considered as point particles for the present purpose, thus allowing the use of classical equations of motion.

Wannier (1953) used phase-space arguments, and related the ionization cross section to the volume of phase space available for double escape. The lower the value of E, the nearer the system must stay to the Wannier ridge for double escape to be possible, and so the volume of phase space corresponding to ionization becomes smaller. In the absence of correlations between the motion of the two electrons (in particular, in the absence of the instability in α), the available phase space, and hence the cross section, is proportional to E. The instability in α becomes important at low values of E, since the system then has a long time in which to roll off the ridge and fall into one of the valleys, thereby removing flux from the ionization channel. The resulting ionization cross section therefore starts at threshold more slowly than linearly. Wannier found the dependence

$$\sigma \sim E^n, \tag{8}$$

where

$$n = \tfrac{1}{4}\{(100Z-9)/(4Z-1)\}^{\frac{1}{2}} - \tfrac{1}{4}. \tag{9}$$

For the process (1), $Z = 1$ and hence $n = 1{\cdot}127$. The phase-space distribution of the initial state of the system (where R is small and the behaviour is not classical) was found not to affect this result, provided that no strong selectivity exists in this distribution (the quasi-ergodic hypothesis). The Wannier law (9) has been confirmed by the semi-classical treatment of Peterkop (1971), the quantum-mechanical treatments of Rau (1971) and Klar and Schlecht (1976), and more recently by Peterkop and Liepinsh (1981). The law applies to all spin and angular momentum configurations of the two outgoing electrons except the $^3S^e$ and $^1P^e$ configurations (Greene and Rau 1982). For these two configurations the wavefunction is necessarily antisymmetric with respect to exchange of the radial distances of the two electrons, which implies that there is a node in the wavefunction at the Wannier point, which in turn causes the exponent n to be larger ($3{\cdot}881$) than that given by equation (9).

If we think of the processes of electron-impact excitation and ionization in terms of the evolution in time of an initially localized wave-packet formed by the impact, we see that the part of the wave-packet corresponding to ionization is the part that remains on or near the Wannier ridge. The radial correlation instability causes a reduction in the amplitude of this part near threshold, making the value of n in

equation (8) slightly greater than unity. We see also that the two electrons are highly correlated in the process of near-threshold ionization, in the sense that they must maintain the condition $r_1 \approx -r_2$ for as long as $R \lesssim R_c$.

The smallness of the difference $n-1$ makes experimental confirmation of the law difficult. The first attempts were measurements of the total cross section for electron-impact ionization of atoms (see e.g. Marchand *et al.* 1969 for references). Marchand *et al.* found that $n = 1{\cdot}16 \pm 0{\cdot}03$, but this type of result was not generally regarded as definitive because of the effects of the finite energy spread of the incident electron beam. More recently a photodetachment experiment using a relativistic H^- beam (Bryant *et al.* 1981) has yielded $n = 1{\cdot}09 \pm 0{\cdot}11$.

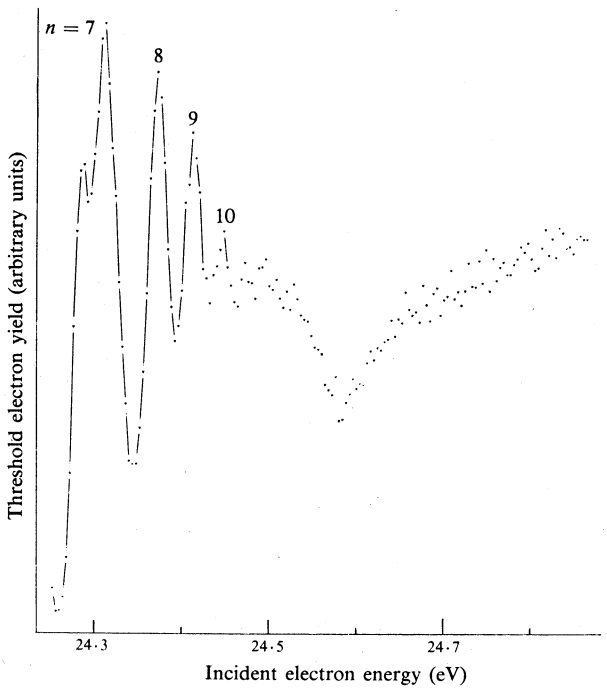

Fig. 2. Yield of very low-energy electrons resulting from electron–helium impact. [S. Cvejanović, personal communication.]

Two experiments of a different type were carried out by Cvejanović and Read (1974). In the first experiment they measured the difference in flight times of the two outgoing electrons, and were thus able to study the energy and angular correlations of the electrons. They confirmed the prediction of the Wannier theory (see also Vinkalns and Gailitis 1967; Peterkop and Liepinsh 1981) that the distribution in θ_{12} becomes more strongly peaked around 180° as the excess energy E is decreased. They confirmed also (within the experimental errors) that the energy-distribution function of each electron is uniform. This result is relevant to the interpretation of their second experiment, in which a partial ionization yield, namely the yield of very slow electrons (having an energy less than E_m, where E_m is ~ 20 meV), was measured. This yield is proportional to the total ionization cross section ($\sim E^n$) times the probability that one of the electrons has an energy less than E_m ($\sim E_m/E$), giving for the partial ionization cross section

$$\sigma_p \sim E^{n-1}. \tag{10}$$

This technique therefore results in a measurement of the difference $n-1$ rather than n itself, thus providing a definitive test of whether or not n is different from unity.

The original measurement by Cvejanović and Read (1974) has been repeated by Cvejanović (personal communication) with better resolution of the incident electron energy (20 meV), and a lower value of E_m (approximately 10 meV). His spectrum is shown in Fig. 2. A detailed analysis of the energy dependence of the yield in the region above the ionization energy (Cvejanović and Read 1974) gives the experimental result

$$n-1 = 0{\cdot}131 \pm 0{\cdot}019, \tag{11}$$

providing a convincing verification of the Wannier law. A similar experiment was carried out later by Spence (1975), using a trapped-electron technique. More recently Pichou *et al.* (1978) have made a more detailed study of electron-impact ionization of helium, and have shown that the energy distribution of the outgoing electrons is uniform up to 3·6 eV above threshold.

(c) *Threshold Excitation*

The part of the spectrum of Fig. 2 that lies below the ionization energy (i.e. $\leqslant 24{\cdot}588$ eV) is also of relevance to the correlations that can exist between two slow electrons, as pointed out by Fano (1974). The peaks in the spectrum correspond to the threshold excitation of Rydberg states of helium. These states have large radii ($\sim n^2$ a.u.) and can only be produced when it is possible for one electron to reach these large distances while the other recedes to infinity. There is time therefore for the instability in α to make itself felt, implying the necessity for the appropriate correlated motion of the two electrons which thus causes a reduction in the threshold excitation yield. As in threshold ionization, the reduction in yield is particularly large when both the electrons have a final kinetic energy which is small, and since the free electron necessarily has a very small kinetic energy in the threshold technique this implies that the bound electron should be in a Rydberg orbital having a high value of n. The influence of long-range electron–electron correlations is therefore similar above and below the ionization energy, and we see from Fig. 2 that there is an approximately symmetric cusp-like dip in the yield of slow electrons at the ionization energy. The symmetry is spoiled only by the discrete nature of the excitation peaks.

The fact that threshold excitation of high-n states occurs only when the two electrons remain in the vicinity of the Wannier ridge for a sufficiently long time implies that the two electrons are correlated in angle, being confined to values of θ_{12} near to 180°. This angular correlation implies in turn that the angular momenta $l_1\hbar$ and $l_2\hbar$ of the two electrons tend to be high, since the sharply peaked function $P(\theta_{12})$ can be decomposed into Legendre polynomials of high order (in a way analogous to the decomposition of a sharp time pulse into sinusoidal components of high frequency). The angular momenta of the excited and outgoing electrons tend of course to be oppositely directed since the total angular momentum of the system remains small. In fact the Wannier theory implies (Fano 1974) that the maximum angular momentum l_m of the individual electrons is proportional to $E^{-\frac{1}{4}}$, where E is now the binding energy of the excited high-n state. Since $E \propto n^{-2}$, we see that $l_m \propto n^{\frac{1}{2}}$. The fact that the excited atoms have angular momenta from 0 to l_m, as

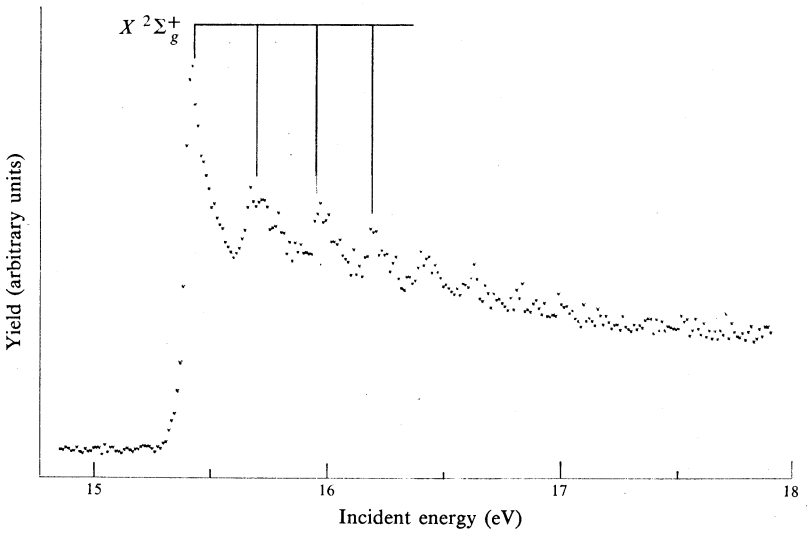

Fig. 3. Yield of metastable H_2 molecules in Rydberg states having n in the range from approximately 31 to 48, resulting from electron impact on H_2, as a function of the impact energy. [Hammond *et al.* 1982*a*.]

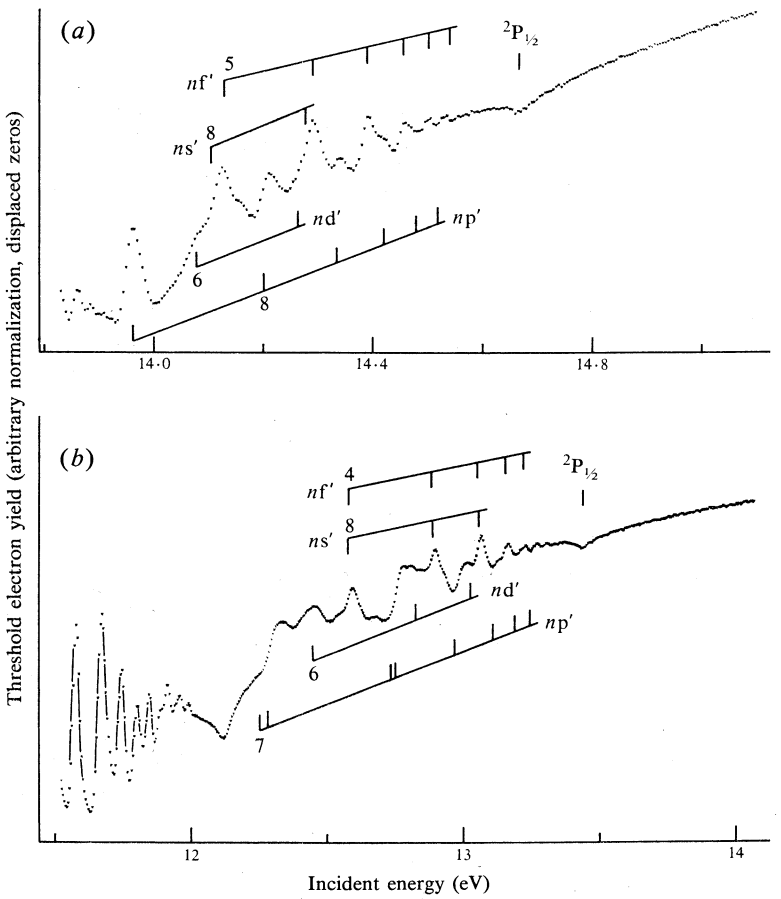

Fig. 4. Threshold excitation spectra of (*a*) krypton and (*b*) xenon. [Hammond *et al.* 1982*b*.]

do the outgoing slow electrons, is in stark contrast to the familiar Wigner threshold law, which gives the energy dependence

$$\sigma \propto E^{l+\frac{1}{2}}, \tag{12}$$

when the residual atom is neutral and the scattered electron has angular momentum $l\hbar$. The Wigner law implies therefore that the scattered electrons would predominantly have $l = 0$ at threshold. The origin of this discrepancy is that long-range correlations are ignored in Wigner's analysis.

The experimental verification of this correlation effect in threshold excitation is made difficult by the fact that the high-l excited states are not easily distinguished from the accompanying low-l states. Heideman *et al.* (1980) have employed optical selection by observing the decay photons, but have been able to do this only for $n \leqslant 6$. Tarr *et al.* (1980) have employed a different method to isolate the high-l states. They have studied near-threshold electron-impact excitation of H_2 and N_2, and have exploited the fact that low-l states of molecules tend to have shorter lifetimes than high-l states of the same n value, since the low-l states can decay more easily by predissociation or autoionization. The high-n high-l states are therefore detected by allowing them to travel along a flight path, at the end of which they are field-ionized and detected. The low-l states tend to decay before reaching the end of the flight path. The energy resolution is poor (350 meV), but there is clear evidence of strong threshold peaks for high-l states. The existence of these threshold peaks has recently been confirmed by the high-resolution measurements of Hammond *et al.* (1982*a*). Fig. 3 shows an example of the yield of Rydberg states of H_2 having n from approximately 31 to 48. Such states exist below each of the vibrational levels of H_2^+. It can be seen that the cross sections for exciting these high-n states are strongly peaked at threshold.

More direct evidence in support of Fano's (1974) prediction comes from high-resolution threshold excitation measurements of krypton and xenon (Hammond *et al.* 1982*b*). These atoms are used because Rydberg states of different l values are separated in energy from each other more than they are in helium. Fig. 4 shows the yield of low-energy ($\lesssim 10$ meV) scattered electrons as the incident electron energy is varied between the $^2P_{3/2}$ and $^2P_{1/2}$ ionization limits. The known energies of the ns', np', nd' and nf' Rydberg series (obtained from optical studies) are indicated. It can be seen that as the $^2P_{1/2}$ ionization limit is approached the peaks assigned to the higher-l states tend to become more intense than those of the lower-l states. In other words, for those krypton or xenon atomic states that have approximately the same binding energy E to the $^2P_{1/2}$ ion core, the states of high l seem to be increasingly more easily excited by near-threshold electron impact, as E becomes smaller, than those of lower l. The near degeneracy of the ns' and nf' series of xenon introduces a slight complication, as do the possible presence of post-collision interactions and the possible influence of the Wannier-ridge resonances (see Section 4), but it seems reasonable to conclude that these observations provide further evidence for the dominance of long-range electron–electron correlations in the excitation process.

3. Correlations in Negative Ion Resonances and Doubly Excited States

(*a*) *Classification Problems*

Perhaps the most familiar doubly excited states are those observed by Madden and Codling (1963) in helium, using synchrotron radiation for the first time. Below

the $n = 2$ level of He^+ there are three ^1P series, the strongest of which was seen in the initial work of Madden and Codling. An important point about these and other doubly excited states, as pointed out by Cooper *et al.* (1963), is that the wavefunctions represent strong admixtures of single-particle configurations, and that they therefore cannot be classified in general by single-particle quantum numbers (see e.g. the discussions of Fano and Lin 1975; Lipsky *et al.* 1977; Herrick and Kellman 1980). Numerical calculations, although very accurate (see e.g. Lipsky *et al.* 1977), have been unable to provide meaningful help in understanding the underlying physical structure of these states. Although the $\pm$ classification scheme (Cooper *et al.* 1963) provides some guidance, as do various other classification models (see e.g. Burke and McVicar 1965; Macek 1968; Wulfman 1973; Herrick and Sinanoglu 1975; Lin 1975; Klar and Klar 1980), the nature of the quantum numbers of these and other doubly excited atomic states has still not been firmly established. Two recent group-theoretical approaches, which may result in the closing of this gap in knowledge, are those of Herrick and Kellman (1980) and Iachello and Rau (1981). We shall return to this point at the end of the present section.

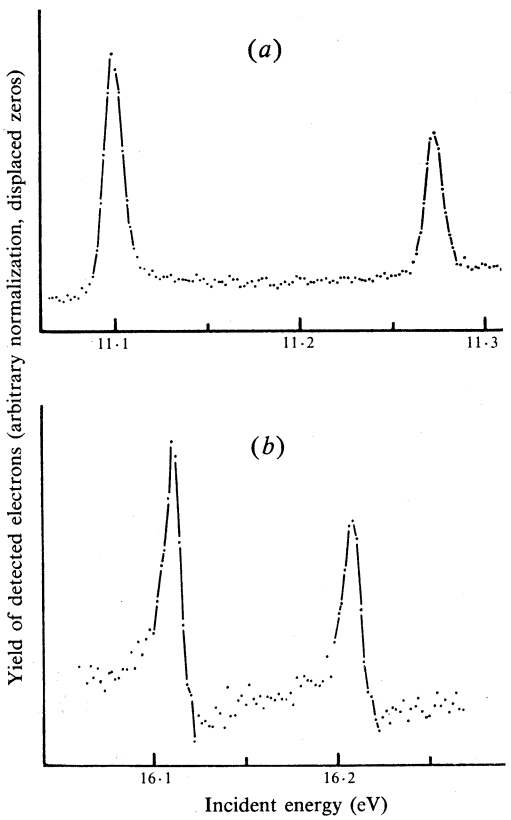

Fig. 5. Electron–atom elastic scattering spectra of (*a*) argon at a scattering angle of 113°; (*b*) neon at a scattering angle of 100°. [Brunt *et al.* 1977*b*.]

A similar area of ignorance is that of the classification of Feshbach resonances. These resonances are short-lived negative ions that can be formed for example by electron–atom impact (see Schulz 1973 for references). Because they essentially consist of two electrons trying to cling to a singly charged positive ion (as opposed to

the doubly charged core of neutral autoionizing atomic states), the mutual correlation of the electrons becomes even more important in determining the behaviour and classification of these states. The resonances therefore represent ideal correlation-dominated systems with which to test two-particle classification schemes.

Fig. 5 (from Brunt *et al.* 1977*b*) shows an example of a high-resolution (12 meV) measurement of the lowest pair of electron-impact resonances in (*a*) argon and (*b*) neon appearing as structures on the elastic-scattering differential cross section. At the time of discovery of these resonances it was suggested (Simpson and Fano 1963) that the structure of the Ne^- pair is that of two 3s electrons coupling to form a closed shell which then couples to the positive ion core in either the $^2P_{3/2}$ or $^2P_{1/2}$ state, giving the classification

$$(1s^2\,2s^2\,2p^5\,{}^2P_{3/2,1/2})\,(3s^2\,{}^1S)\,{}^2P_{3/2,1/2}\,.$$

In this 'external' coupling scheme the binding energy of the $3s^2$ pair to the 'grandparent' ion core is 5·45 eV. Analysis of the spectra of Fig. 5 reveals that for both argon and neon the energy separation of the resonances is *equal* (within the experimental error of ± 1 meV) to that of the grandparent positive-ion states, showing that there is very little magnetic interaction or exchange correlation between the outer two electrons and the inner core. These resonances are therefore examples of nearly pure external coupling.

An alternative coupling scheme is that of sequential (or aufbau) coupling, in which one electron is bound (with an energy of ~ 5 eV) to the ion core to form a parent state to which is added the remaining electron with a very low binding energy ($\sim 0{\cdot}5$ eV). The degree of correlation between the outer electrons is then lower than with external coupling. Since we know that external coupling of an ns^2 pair gives a greater binding energy due to the increased degree of correlation (see next subsection), we may suspect that external coupling will occur also for an $nln'l'$ configuration in which $l \neq l'$. In fact Read *et al.* (1976) and Buckman *et al.* (1982*a*, 1982*b*) have shown that it is possible to interpret qualitatively the positions and widths of many of the higher lying resonances in neon, argon, krypton and xenon in terms of an external coupling scheme for both equivalent and non-equivalent electrons, but clearly more detailed theoretical studies are still required. The external coupling scheme has also been used to interpret the observed He^- resonances (Brunt *et al.* 1977*a*), although here there are additional structures caused by a virtual state near the 2^1S energy, by cusp effects at the energies of excited neutral states, and by the existence of a different type of resonance having the structure of an electron very weakly bound in the polarization potential of an excited state (Nesbet 1978). We must therefore not expect all resonances to be of the external coupling type. Further evidence of external coupling comes from the calculations of Langlois and Sichel (1980) on doubly excited levels of neon.

(*b*) *Modified Rydberg Formula*

At this stage it is worth while to consider what form of electron–electron correlation is implied by external coupling. Read (1977) has considered atoms and ions having a configuration [core]($ns^2\,{}^1S$), and has investigated the consequences of supposing the following: (i) that each *ns* electron partially screens the other from the charge of the core, so that the Coulomb potential outside the core is effectively reduced from

Z/r to $(Z-\sigma)/r$, where σ is a screening parameter; (ii) that the stronger non-Coulombic potential experienced by an electron when it penetrates the core is parametrized by the same quantum defect δ_{ns} that a single ns electron would have in the atom or ion [core](ns). These two suppositions lead to the modified Rydberg formula

$$E([\text{core}]) - E([\text{core}]ns^2) = 2R(Z-\sigma)^2/(n-\delta_{ns})^2 \qquad (13)$$

for the energy with which the externally coupled ns^2 electrons are bound to the core, where R is the Rydberg energy (13·606 eV). The quantum defect used in this formula has to be rendered free of the effects of magnetic interactions and exchange correlations by taking the appropriate energy averages (see Read 1977 for details).

Table 1. Application of modified Rydberg formulae (13), (16) and (17) to configurations [core]ns^2 where n has its lowest value

E and E_I are the energies of the states [core]ns^2 and [core] respectively

Atom	Config-uration	Parameter					Δ (%) using	
		Z_{core}	E (eV)	E_I (eV)	δ_{ns}	σ^A	eqn (16)	eqn (17)
H^-	$1s^2$	1	0	14·355	0	0·274	6·58	0·81
He	$1s^2$	2	0	79·005	0	0·296	5·47	0·59
He^-	$1s\,2s^2$	1	19·367	24·588	0·274	0·244	−1·60	−2·45
Li	$1s\,2s^2$	2	56·31	81·032	0·166	0·252	0·22	−1·26
Ne	$2p^4(^3P_2)3s^2$	2	41·87	62·647	1·008	0·259	1·08	−0·11
Ar	$3p^4(^3P_2)4s^2$	2	26·97	43·386	1·758	0·259	0·99	0·20
Be I	$1s^2\,2s^2$	2	0	27·534	0·272	0·261	1·36	−0·37
B II	$1s^2\,2s^2$	3	0	63·087	0·204	0·265	1·13	−0·49
F VI	$1s^2\,2s^2$	7	0	342·35	0·103	0·270	0·64	−0·61
Mg I	$2p^6\,3s^2$	2	0	22·681	1·098	0·263	1·57	0·21
Al II	$2p^6\,3s^2$	3	0	47·277	0·926	0·265	1·19	0·00
Si III	$2p^6\,3s^2$	4	0	78·611	0·804	0·268	0·94	−0·13
Sc X	$2p^6\,3s^2$	11	0	475·43	0·433	0·270	0·38	−0·32
Sr I	$4p^6\,5s^2$	2	0	16·724	2·779	0·259	1·02	0·19
Ba I	$5p^6\,6s^2$	2	0	15·215	3·668	0·256	0·72	0·04
O^-	$(^4S)3s^2$	1	8·78	13·618	1·228	0·253	0·76	0·06
Ne^-	$2p^5(^2P_{3/2})3s^2$	1	16·111	21·565	1·334	0·254	1·12	0·02
Ar^-	$3p^5(^2P_{3/2})4s^2$	1	11·098	15·760	2·193	0·252	0·55	−0·03
Kr^-	$4p^5(^2P_{3/2})5s^2$	1	9·484	14·000	3·165	0·252	0·66	0·17
Xe^-	$5p^5(^2P_{3/2})6s^2$	1	7·900	12·130	4·111	0·255	1·41	1·09
Na^-	$2p^6\,3s^2$	1	0	5·682	1·373	0·256	1·77	0·50
K^-	$3p^6\,4s^2$	1	0	4·842	2·230	0·253	0·90	0·19
Rb^-	$4p^6\,5s^2$	1	0	4·663	3·195	0·253	0·75	0·16
Cs^-	$5p^6\,6s^2$	1	0	4·365	4·131	0·251	0·39	0·01

[A] From equation (13).

The screening parameter σ can be found when all the other parameters in equation (13) are known. Table 1 shows some examples for configurations of the type [core]ns^2 in which n has its lowest possible value. Of more than 50 examples considered, only three give rise to values of σ that lie outside the range $0{\cdot}25 \pm 0{\cdot}02$, and of these, H^- and He have a bare nucleus as the core, while Au^- (not shown in Table 1) has core d electrons which overlap the outer ns^2 electrons. We see therefore that σ is remarkably constant, being usually slightly greater than 0·250 (while the average value is 0·257).

The significance of the value 0·25 is that this is the value that σ has when the system of core plus two electrons exists on or near the Wannier ridge (i.e. when $r_1 \approx -r_2$), since we see from equation (5) that the potential energy is then

$$V_W = -(2\sqrt{2}/R)(Z-\tfrac{1}{4}) = -(2/r)(Z-\tfrac{1}{4}). \tag{14}$$

We see also from Fig. 1 that, because the region surrounding the Wannier point is nearly flat, σ is not greatly changed by the fact that the probability distribution of the two-electron wavefunction is distributed around (rather than at) this point.

The fact that σ is always $\approx 0{\cdot}25$ for [core]ns^2 configurations implies therefore that the two outer electrons have a high degree of correlation, in the sense that they spend most of the time on or near the Wannier ridge, screening each other as little as possible from the positively charged core. This value of σ represents the minimum amount of screening. The maximum value of 0·5 occurs when the two electrons are completely uncorrelated. Another implication of the results shown in Table 1 is that the quantum defect δ_{ns} for a single electron can still be used to parametrize the core when a second electron is present, a fact which will no doubt be of help when two-electron models (see next subsection) are applied to atoms having extended cores.

Also shown in Table 1 is the error

$$\Delta = \{E_B(\text{calc.}) - E_B(\text{exp.})\}/E_B(\text{exp.}) \tag{15}$$

in the calculated binding energy if equation (13) is used with $\sigma = 0{\cdot}25$, i.e.

$$E_B(\text{calc.})/(27{\cdot}212\text{ eV}) = (Z-0{\cdot}25)^2/(n-\delta_{ns})^2. \tag{16}$$

We see that the absolute value of Δ is $<2\%$ for all the atoms considered, except the two-electron atoms H^- and He. This is a remarkable achievement for a formula that contains no variable parameters.

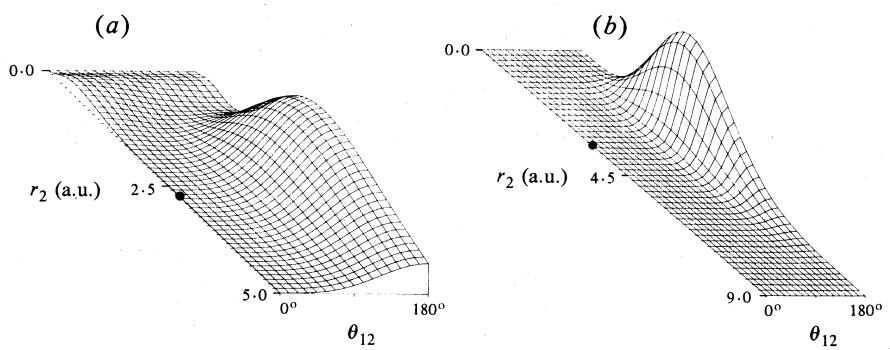

Fig. 6. Conditional probability densities $\rho(r_2, \theta_{12})$ for He**. The dot indicates the position of electron 1: (*a*) $2s^2\ {}^1S_e$ state with $r_1 = 2{\cdot}74\ a_0$, its most probable value; (*b*) $2s2p\ {}^3P^o$ state with $r_1 = 3{\cdot}5\ a_0$, its most probable value. [Yuh *et al.* 1981.]

To obtain an even closer fit to the experimentally measured binding energies we have added to equation (13) a further term (the justification for which will be discussed in Section 3*d* below), to give the expression

$$E_B/(27{\cdot}212\text{ eV}) = \{(Z-\sigma)^2/(n-\delta_{ns})^2\} - c\{(Z-\sigma)^{3/2}/(n-\delta_{ns})^3\}, \tag{17}$$

where c is a constant. The best fit is obtained with $\sigma = 0{\cdot}23$ and $c = 0{\cdot}09$, and the resulting percentage errors are shown in the last column of Table 1. The quality of this fit is even more remarkable, since of the many and varied atoms considered (spanning Z_{core} from 1 to 11, n from 1 to 6, and δ_{ns} from 0 to 4·1) the error in using equation (17) is rarely greater than 1%, even when the core is a bare nucleus.

(*c*) *Calculational and Theoretical Studies*

Rehmus *et al.* (1978) and Yuh *et al.* (1981) have investigated the electron correlations that exist in doubly excited states of helium by expressing $|\Psi|^2$ as a function of r_1, r_2, θ_{12} and two other coordinates θ_1 and θ_2, and then averaging over the redundant coordinates θ_1 and θ_2 to obtain the density function $\rho(r_1, r_2, \theta_{12})$. One of these results is shown in Fig. 6, in which the density functions of the $2s^2\ ^1S$ and $2s2p\ ^3P$ states are plotted as a function of r_2 and θ_{12}. It can be seen that these wavefunctions are localized near the Wannier point. Analogous strong correlations are found in the wavefunctions of other doubly excited states of helium. It is also interesting to note that an analogous spatial correlation seems to exist in fully or partially filled p shells (Read 1977).

Let us now consider the various theoretical attempts to account for the correlations in doubly excited states of the atoms H^- and He. The main task is of course to find a separation of coordinates that will allow the formulation of the underlying selection rules and quantum numbers referred to at the beginning of this section.

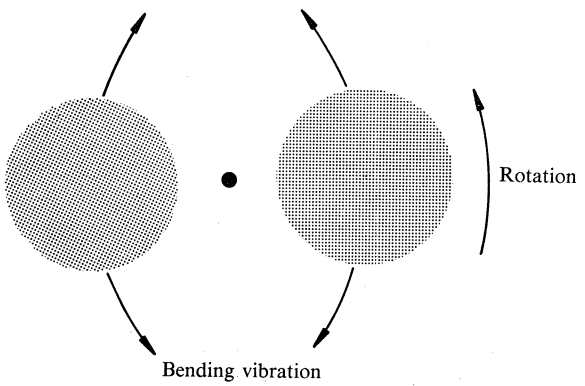

Fig. 7. Schematic representation of the rotational–vibrational collective interpretation of supermultiplet classifications of intrashell levels of two-electron atoms. The two electron clouds and the ion core form a linear *XYX* structure that vibrates and rotates.

In several of the theoretical studies (see e.g. Macek 1968; Lin 1975; Klar and Klar 1980; Greene 1981; Watanabe 1982) hyperspherical coordinates have been used, with the implicit assumption that the 'breathing' motion in the scale distance R is significantly slower than the motion in α and θ_{12}. This assumption allows R to be treated as the analogue of the inter-nuclear separation of a diatomic molecule, and α and θ_{12} as the analogues of the electronic coordinates of the molecule, giving a Born–Oppenheimer type of separation. The eigenvalues of the Hamiltonian at constant values of R are therefore regarded as potentials which determine the motion in R. As in the evaluation of molecular energy levels, potential energy functions are calculated and then used to find the total atomic eigenenergies. This approach leads to reasonably accurate eigenenergies, and is also able to explain qualitatively the observed differences in transition strength in terms of the shape of the low-R repulsive part of the potential curves: the curves which extend to the lowest values of R give wavefunctions which have the greatest overlap with the target wavefunction and

hence have the highest absorption strength. In other words, the transition strength differences are ascribed in this model to a dynamical effect, rather than to the existence of selection rules.

Some success has been obtained also with other types of coordinate separation (see e.g. Burke and McVicar 1965; Wulfman 1973; Herrick and Sinanoglu 1975). A promising approach is that recently evolved by Kellman and Herrick (1978) and Herrick and Kellman (1980), who have considered the classification of doubly excited states of helium in which both electrons have the same principal quantum number n. Their work is based on decompositions of the group to which two-electron atoms belong, but their results can be interpreted in terms of a simple model and its associated quantum numbers. The model is depicted in Fig. 7. The shaded areas represent the regions in which the two electrons reside for most of the time, with one electron on each side of the nucleus. This structure is similar to that of a linear XYX triatomic molecule, and so there are additional 'vibrational' and 'rotational' motions, as indicated in the figure. The electron wavelengths are of course comparable with the mean electron–nucleus separation, which gives the electrons a large spatial extent and makes the 'molecule' far less rigid than a real triatomic molecule. It therefore bends easily in any plane through the mean molecular axis, and since this bending vibration has a degeneracy of two it can also give rise to angular momentum about the mean axis. Symmetric and antisymmetric vibrational motions are incorporated into the 'internal' structure shown in Fig. 7. Finally, rotational motion is superimposed on the internal and bending motions.

The energy levels given by this model are therefore analogous to those of a linear triatomic molecule, namely

$$E = E_{\text{int}} + \omega(v+1) + B_e\{J(J+1) - l^2\}, \tag{18}$$

where E_{int} is the internal energy, ω the vibrational constant, B_e the rotational constant, v the vibrational quantum number, J the total angular momentum quantum number and l represents the component of angular momentum about the mean axis. The 'molecular' quantum numbers v, J and l are related to the 'atomic' quantum numbers K, T and I that label the subgroups considered by Herrick and Kellman. Group-theoretical considerations impose certain constraints and cut-offs on the atomic, and hence the molecular, quantum numbers. In addition, the requirement that the wavefunction be antisymmetric with respect to exchange of the two electrons determines the allowed value of the total electron spin S for given parity Π and quantum number l. The resulting values of the atomic terms for the $n = 3$ shell of helium are shown as a set of supermultiplets in Fig. 8*a*. Each supermultiplet, corresponding to a fixed value of $J-l$, forms a diamond structure. The corresponding energy levels are plotted in the same form in Fig. 8*b*. Because of the lack of experimentally measured energies it has been necessary to use accurately calculated values.

We see from Fig. 8*b* that the proposed supermultiplet classication reveals a high degree of regularity in the energy spectrum. Other schemes of classification (for example, in terms of the independent-electron quantum numbers l_1 and l_2) are less successful in this respect. The classification also corresponds well with the energy level formula (18). Within each supermultiplet we see vibrational series of approximately equi-spaced levels, and we see also that when v is non-zero the bending motion can contribute angular momentum l. Levels having the same v but different l (within a supermultiplet) are nearly degenerate, which explains for example the triplet

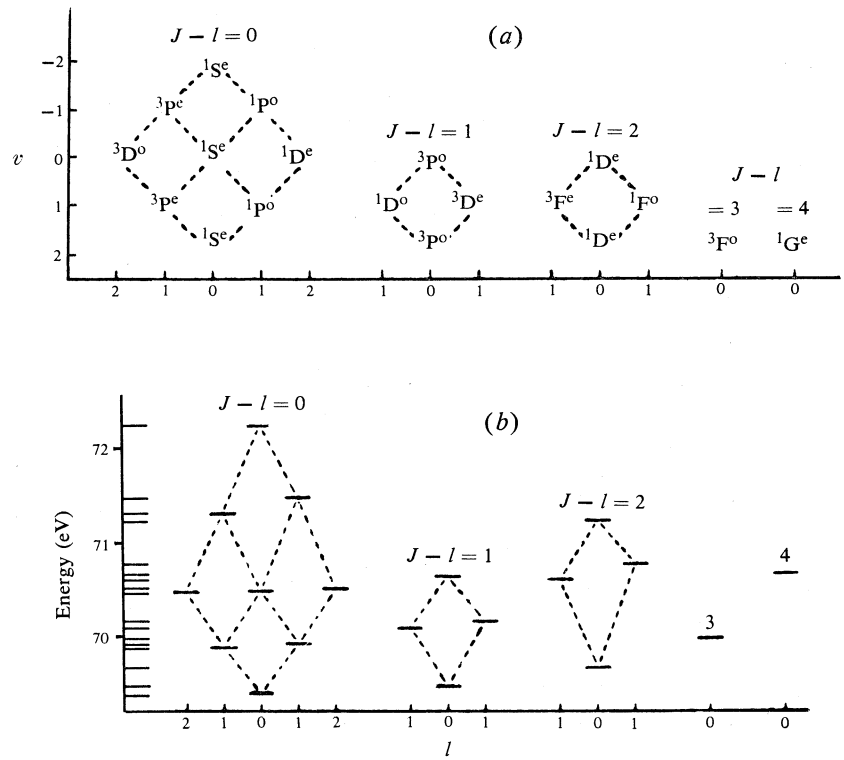

Fig. 8. (*a*) Supermultiplet classification of doubly excited states of helium in the $n = 3$ shell; (*b*) calculated energies according to the same classification. [Herrick and Kellman 1980.]

of nearly degenerate levels near 70·5 eV. The lowest levels of the supermultiplets reveal the purely rotational component, their energies being approximately proportional to $J(J+1)$. This classification scheme seems to indicate therefore a new and useful separation of coordinates into internal, vibrational and rotational coordinates.

More recently a different group-theoretical approach has been developed by Iachello and Rau (1981). They show that matrix elements of the Coulomb interaction for doubly excited ^{1}S states can be approximated by a constant plus a pairing term, and that the pairing term gives rise to a highly correlated state similar to a Cooper pair in an electron gas. They show also that the correlated state may be identified with the state that leads to the Wannier threshold law for the escape of two electrons from a Coulomb core. Clearly the understanding of electron–electron correlations in atoms such as doubly excited helium is developing at a fast pace, and the ultimate amalgamation of the various approaches, and also their application to heavier atoms and to resonances, is awaited with interest.

(*d*) *Semi-empirical Formulae*

The success of the modified Rydberg formula (16) in fitting the binding energies of configurations [core]ns^2, where n has its lowest value, and the insight offered by the Herrick and Kellman (1980) rotor model in describing the structure of the higher

Table 2. Atomic configuration, quantum numbers and energies in rotor model

Configuration	v	J	l	Energy (a.u.)	Configuration	v	J	l	Energy (a.u.)
$(s^2+p^2+d^2+\ldots)\,{}^1S^e$	0	0	0	ω	$(p^2+d^2+f^2+\ldots)\,{}^3P^e$	1	1	1	$2\omega+B$
$(sp+pd+df+\ldots)\,{}^3P^o$	0	1	0	$\omega+2B$	$(sp+pd+df+\ldots)\,{}^1P^o$	1	1	1	$2\omega+B$
$(sd+p^2+d^2+\ldots)\,{}^1D^e$	0	2	0	$\omega+6B$	$(pd+df+fg+\ldots)\,{}^3D^o$	2	2	2	$3\omega+2B$
$(sf+df+fg+\ldots)\,{}^3F^o$	0	3	0	$\omega+12B$	$(s^2+p^2+d^2+\ldots)\,{}^1S^e$	2	0	2	$3\omega+6B$
					$(sd+p^2+d^2+\ldots)\,{}^1D^e$	2	2	2	$3\omega+2B$
					$(pd+df+fg+\ldots)\,{}^1D^o$	1	2	1	$2\omega+5B$
					$(sd+pf+dg+\ldots)\,{}^3D^e$	1	2	1	$2\omega+5B$

Table 3. Measured and fitted values of vibrational (ω eV) and rotational (B eV) constants in rotor model

Atom	n	ω_m	ω_{fit}	B_m	B_{fit}	Atom	n	ω_m	ω_{fit}	B_m	B_{fit}
H^-	2	0·52	0·92	0·090	0·151	B II	2	8·37	8·66	2·32	2·70
	3		0·27	0·055	0·045	Mg	3	4·40	3·73	1·36	0·93
He	2	1·84	3·20	0·24	0·80	Al II	3	7·23	5·63	2·33	1·76
He^-	2		1·43	0·31	0·24	Si III	3	9·91	7·52	3·28	2·74
Li	2		4·16	0·77	1·04	Sc X	3		22·74	10·01	13·99
Be	2	4·98	4·97	1·36	1·24						

energy configurations [core]$ns\,np$, [core]np^2 etc., give encouragement to the task of combining these two models to give energy formulae that fit the wider class of states.

In Table 2 we show the possible configurational mixtures of the lower lying rotor states depicted in Fig. 8, together with their corresponding vibrational–rotational energies, as given by equation (18). By including the effects of anharmonicity, centrifugal distortion and rotational–vibrational coupling the energy becomes (Kellman and Herrick 1980)

$$E = E_{int}+\omega(v+1)-x(v+1)^2+\{B-\alpha(v+1)\}\{J(J+1)-l^2\} + Gl^2-D\{J(J+1)-l^2\}^2, \tag{19}$$

and although Kellman and Herrick show that for helium the constants x, α, G and D are not always significantly smaller than ω and B, we shall ignore the extra terms for the time being. Using the data summarized by Read (1977), values of B for 11 different atoms can be deduced from the energy differences of their [core]($ns^2\,{}^1S$) and [core]($ns\,np\,{}^3P$) terms, and similarly values of ω for seven of these atoms can be deduced from the energies of the [core]($ns\,np\,{}^1P$) terms, or from the means of these and the energies of the [core]($np^2\,{}^3P$) terms, where available (see Table 3). To parametrize these results we start with the expressions given by Kellman and Herrick (1980) for the values of ω and B (in a.u.) when the electron–core separations both have the fixed value r:

$$\omega = 1/2r^{3/2}, \tag{20}$$

$$B = 1/4r^2. \tag{21}$$

Now at the Wannier point the potential energy of the system is given by equation (14), and from the virial theorem (see e.g. Cowan 1981) the mean potential energy is related to the binding energy by

$$\bar{V} = -2E_B. \tag{22}$$

Putting

$$\bar{V} \approx \bar{V}_{\mathrm{W}} = -2(Z-\tfrac{1}{4})\langle r^{-1}\rangle , \tag{23}$$

where $\langle r^{-1}\rangle$ denotes the mean value, and replacing the screening constant 0·25 by σ, and also using equation (13) to parametrize E_{B}, we now obtain

$$\langle r^{-1}\rangle \approx (Z-\sigma)/(n-\delta_{ns})^2 , \tag{24}$$

and hence

$$\omega \approx \tfrac{1}{2}\langle r^{-1}\rangle^{3/2} \approx (Z-\sigma)^{3/2}/2(n-\delta_{ns})^3 . \tag{25}$$

Similarly, or by making use of the expression for $\langle r^{-2}\rangle$ for hydrogenic atoms (Cowan 1981), the approximate parametrization of B becomes

$$B \approx (Z-\sigma)^2/4(n-\delta_{ns})^4 . \tag{26}$$

To fit the measured values given in Table 3 the proportionality constants in equations (25) and (26) have been treated as adjustable, but σ has been fixed at the value that appears in equation (17) (namely 0·23). The best fits, given in Table 3, are obtained with the expressions

$$\omega_{\mathrm{fit}}/(27{\cdot}212\ \mathrm{eV}) = 0{\cdot}4(Z-0{\cdot}23)^{3/2}/(n-\delta_{ns})^2 , \tag{27}$$

$$B_{\mathrm{fit}}/(27{\cdot}212\ \mathrm{eV}) = 0{\cdot}075(Z-0{\cdot}23)^2/(n-\delta_{ns})^3 . \tag{28}$$

We see that in both cases the proportionality constants are less (by factors of 0·8 and 0·3 respectively) than those appearing in equations (25) and (26). These reductions are presumably due, at least in part, to the presence of the higher terms in equation (19).

Since the term [core]ns^2 has the zero-point vibrational energy $\hbar\omega$ (note that the bending mode is doubly degenerate), it seems appropriate to add this to the binding energy of the [core]ns^2 term before fitting with the modified Rydberg formula. Treating the proportional constant for the vibrational energy as an adjustable parameter again, we obtain equation (17) which, as already noted, gives an excellent fit to the measured binding energies. The constant c that gives the best fit is 0·09, which is smaller than that expected from equation (27) by a factor of 0·225. It seems therefore that a part of the zero-point energy is already incorporated in some sense into the electronic energy $(Z-\sigma)^2/(n-\delta_{ns})^2$. The fact that the screening constant which gives the best fit is 0·23 rather than 0·25 also needs to be considered. We see from equation (5) that the quadratic term in α in the expansion of V near the Wannier point can be combined with the screening constant 0·25 at the Wannier point to give an effective screening constant

$$\sigma = 0{\cdot}25-\tfrac{1}{8}(12Z-1)\langle(\alpha-\tfrac{1}{4}\pi)^2\rangle . \tag{29}$$

To reproduce $\sigma = 0{\cdot}23$ requires

$$(\alpha-\tfrac{1}{4}\pi)_{\mathrm{rms}} = 0{\cdot}115/(Z-\tfrac{1}{12})^{\frac{1}{2}} . \tag{30}$$

The wavefunction density plots of Lin (1982) show that the range of α over which ns^2 states extend is at least as large as that given by equation (30). Note that the quadratic term in θ_{12} in equation (5) is already allowed for in that it gives rise to the bending vibration.

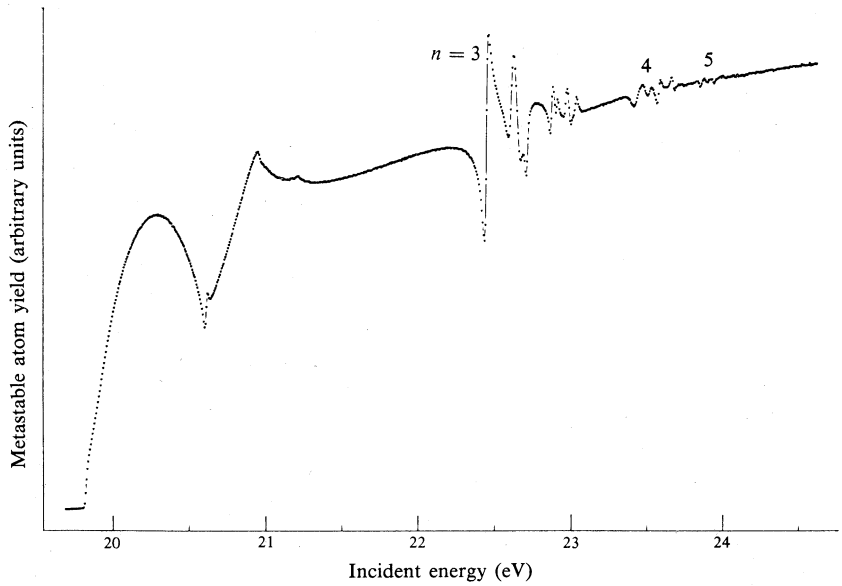

Fig. 9. Yield of metastable (2^3S and 2^1S) helium atoms resulting from electron impact on helium as a function of incident electron energy. The energy resolution is 15 meV. [Buckman *et al.* 1982*c*.]

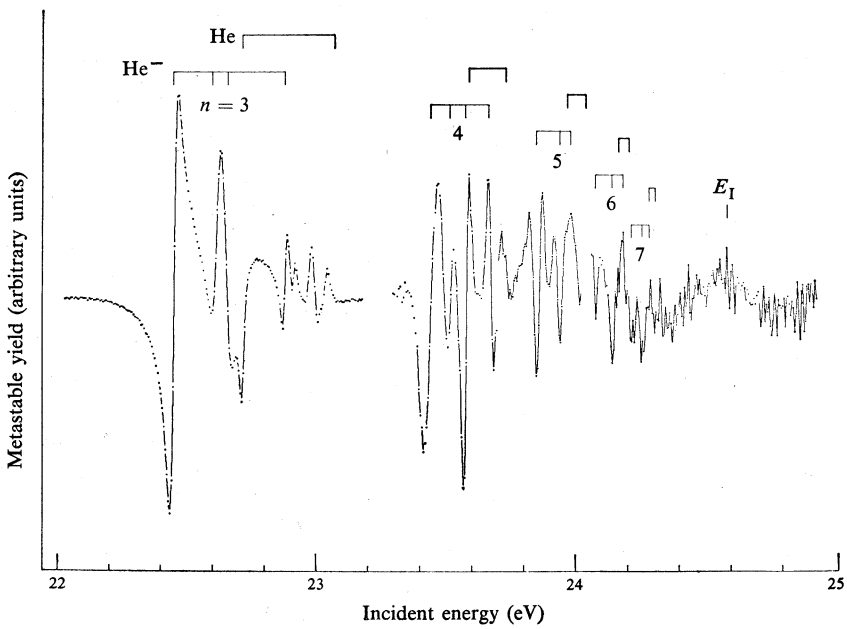

Fig. 10. Yield shown in Fig. 9, but taken over four restricted energy regions with improved statistical accuracy. The relative normalization of the four regions is arbitrary. The energies of the $1snS$ ^3S and $1snd$ ^1D states of helium are indicated for n = 3–7 (to show the ranges of energies covered by the $1sn$ multiplets). The energies of the more prominent He^- resonances as well as the ionization energy E_I are also indicated. [Buckman *et al.* 1982*c*.]

4. 'Wannier-ridge' Resonances

(*a*) *Experimental Evidence*

In Section 2 we discussed the effects of long-range correlations between two unbound electrons (as exemplified in the process of near-threshold electron-impact ionization) and between a bound and an unbound electron (as exemplified in the process of near-threshold electron-impact excitation of atomic states of high l). The typical energy of electrons for which such effects are important is $\pm E$, where $E \lesssim 0{\cdot}5$ eV. In Section 3 we were concerned with the correlations that exist in atomic and resonance states in which the two excited electrons are in valence or near-valence orbitals, with a combined binding energy to the relevant ion core that is typically a few electron volts. In the present section we are concerned with resonance states for which the binding energy is $\lesssim 0{\cdot}5$ eV, so that both the excited electrons have high values of the principal quantum number n.

Table 4. Observed properties of He^- resonances

Values in parentheses indicate error in last significant figure

n	Observed energies (eV)				1st ^2S
	1st ^2S resonance	^2P resonance	^2D resonance[A]	2nd ^2S resonance[B]	rel. ht[C]
2	19·367(5)				
3	22·450(5)	22·600(10)	22·660(10)	22·881(5)	0·55(1)
4	23·443(5)	23·518(10)	23·579(10)	23·667(5)	0·051(1)
5	23·851(10)	23·907(10)	23·943(10)	23·985(10)	0·018(1)
6	24·079(10)		24·142(10)	24·185(10)	0·0061(4)
7	24·216(10)		24·258(10)	24·284(10)	0·0046(4)
8	24·306(20)				

[A] Second narrow dip.
[B] Final broad peak.
[C] Ratio (peak-to-valley)/mean for the first ^2S resonance in each group.

In recent experiments Buckman *et al.* (1982*c*) have measured the yield of metastable helium atoms (in either the 2^1S or 2^3S states), that result from electron–helium impact, as a function of the incident electron energy. Their results are shown in Fig. 9. The threshold and resonance structures that appear in this excitation function occur in distinct groups, each group being labelled by the appropriate principal quantum number n. For the threshold features (such as those appearing at 20·616 and 20·964 eV) the value of n refers to the principal quantum number of the excited electron in the corresponding excited state of helium (in this example the $1s2s\ ^1S$ and $1s2p\ ^3P$ states at 20·616 and 20·964 eV respectively), whereas for the resonance features the value of n refers to the lower of the principal quantum numbers n_1 and n_2 of the two excited electrons. The lower energy resonances in each group have $n_1 = n_2$, while those at higher energies can have $n_1 \neq n_2$.

The threshold and resonance features in the groups labelled $n = 2$ and 3 have been well studied previously, both experimentally and theoretically (see e.g. Brunt *et al.* 1977*a*; Nesbet 1978; Andrick 1979 and references therein). Of greater interest in the present work are the groups at higher values of n. The existence of these higher lying resonances was first established by Heddle and coworkers (see Heddel

1977 for a summary and references), who measured optical excitation functions of several high-lying states of helium. To study these resonances at high resolution in the metastable excitation function, Buckman *et al.* (1982*c*) have used a greatly improved sensitivity since the features are very small compared with the non-resonant cross section. Fig. 10 shows in greater detail the groups with n from 3 to 7.

The energies and l values indicated in Fig. 10 (and included also in Table 2) for four prominent resonances in the $n = 3$ group are those established by angular distribution studies (Andrick 1979). The calculations of Nesbet (1978) indicate that the lower three of these resonances are of the intrashell type (for which $n_1 = n_2$), having the dominant configurations $1s\,3s^2\ ^2S$, $1s\,3s\,3p\ ^2P$ and $1s\,3s\,3d\ ^2D$ respectively, while the remaining one is of the intershell type. These same four features appear to be present also in the group having $n = 4$. For each of the groups where n is 5, 6 and 7, the lowest ^2S feature appears as a narrow dip and is clearly discernible (although it is much less so for $n = 8$), and also the energies of two other prominent features in each group, namely a second narrow dip and a final broad peak, can be confidently established. These energies are indicated in Fig. 10 and given in Table 4. Energies of the $1snS\ ^3S$ and $1snd\ ^1D$ states of He are also shown in Fig. 10, representing the span of neutral-state energies at each value of n. The energies obtained for some of these resonances by Heddle and coworkers (see Heddle 1977), at a significantly lower resolution, are on the whole consistent with those given in Table 4.

The high n^2 resonances in He^- have also been observed recently in electron-impact excitation functions of various states of helium (Hammond *et al.* 1982*b*). Some examples of these excitation functions are shown in Fig. 11. As one might expect, resonances with a given value of n appear most strongly in excitation functions of the states that have the principal quantum number $n-1$. This was established also by the optical excitation studies of Heddle (1977). Work is proceeding (Cvejanović, personal communication) on the behaviour of these resonance structures in electron-impact excitation functions as a function of the angle of scattering and of the excitation channel.

Some qualitative conclusions can be drawn immediately from the spectrum shown in Fig. 11 by comparing the positions of the multiplets of singly excited states of He with those of the doubly excited states of He^-. For the singly excited states the excitation energies are well approximated by the Rydberg formula

$$E_{nl} = E_I - RZ_{\text{core}}^2/(n-\delta_{nl})^2\,, \tag{31}$$

where E_I is the ionization energy and where the quantum defect δ_{nl} converges to a constant at high values of n (i.e. $n \gtrsim 4$); for example, for the ^3S and ^1D states, δ converges to 0·30 and ≈ 0 respectively. The energy separation between two states that differ in n by unity but have the same symmetry is

$$E_{(n+1)l} - E_{nl} \approx 2RZ_{\text{core}}^2/(n-\bar{\delta}_{nl})^3\,, \tag{32}$$

which is proportional to n^{*-3} at high n (where $n^* = n-\delta$). Similarly the energy separation between two states that have the same n but different symmetry is

$$E_{nl} - E_{nl'} \approx 2RZ_{\text{core}}^2(\delta_{nl'} - \delta_{nl})/(n-\bar{\delta})^3\,, \tag{33}$$

which again becomes proportional to n^{*-3}. The energy span of each multiplet and the energy separation of neighbouring multiplets are therefore both proportional to n^{*-3} (Fano and Cooper 1968), and the ratio of span to separation is a constant.

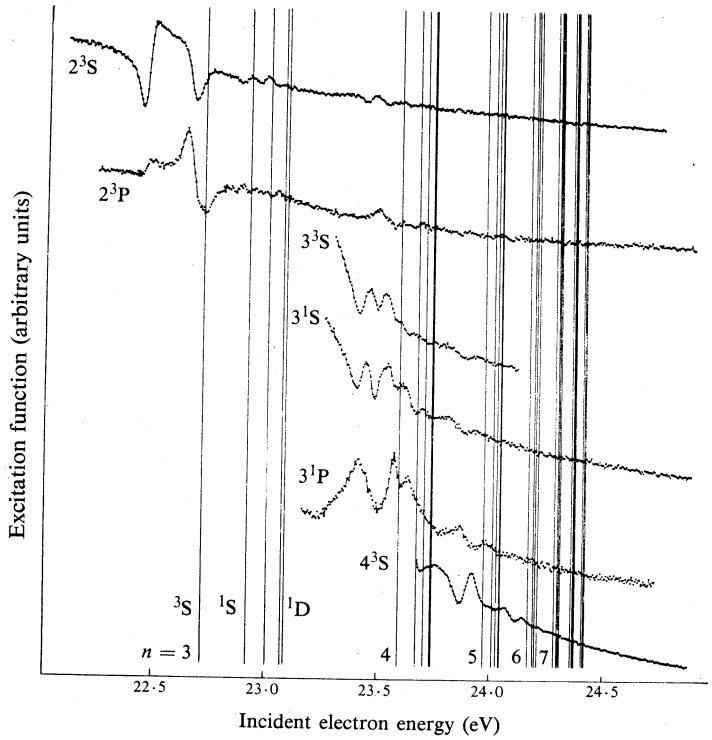

Fig. 11. Electron-impact excitation functions of various states of helium in the region below the ionization potential. The relative normalizations are arbitrary. The vertical lines show the energies of excited states of helium. [Hammond *et al.* 1982*b*.]

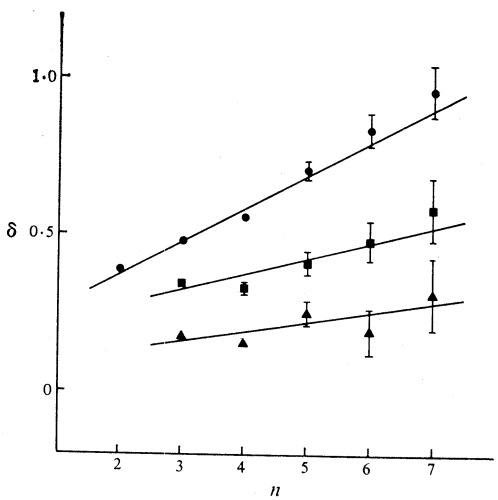

Fig. 12. Quantum defects (obtained from the one-electron formula 31) of the observed He^- resonances plotted as a function of the principal quantum number n of the two excited electrons. The circles correspond to the first ^2S resonances, the squares to the ^2D resonances or (in the case of the higher n values) the second narrow dip in each n group, and the triangles to the second ^2S resonances or the final broad peak in each group.

This is the behaviour of the singly excited state energies that are indicated in Fig. 10. In contrast we see from this figure that the ratio of multiplet energy span to multiplet separation is *not* a constant for the He^- resonance states. Indeed it is clear that the multiplets start to overlap at $n \gtrsim 8$.

Another way of underlining the essential difference in character between the multiplets of He* and He^{-}** is to try to apply the single-electron Rydberg formula (31) to the energies of the He^- states. The resulting values of δ_{nl} are shown in Fig. 12. We see that these effective single-electron quantum defects do *not* converge to constant values at high n. This piece of evidence clearly indicates therefore that *two* excited electrons are involved, and that these electrons are strongly correlated.

(*b*) *Interpretation*

Fano (1980) has recently pointed out a connection between the behaviour of an atomic Rydberg electron in a strong magnetic field, giving rise to Landau standing waves, and the behaviour of two slow electrons escaping from the field of an atomic ion in the process of near-threshold electron-impact ionization of an atom. In both examples there is unstable motion along a potential ridge. In the case of two electrons escaping from an atomic field the ridge is the Wannier ridge at $\boldsymbol{r}_1 = -\boldsymbol{r}_2$, where the potential is given by equation (14). Fano (1980) has suggested that, in analogy with the formation of Landau standing waves, the form of the two-electron potential ridge might give rise to series of quasi-standing wave patterns formed by reflection of the wave-packet representing the two-electron system. The wave-packet propagates along the ridge and is reflected when the kinetic energy becomes zero (i.e. at the radius $r_{1,2}$ at which V is equal to the total energy of the system). These standing waves could manifest themselves as resonances in electron–atom scattering at energies near to, and below, the ionization energy. We believe that some of the resonances seen in the present work, in particular the lower energy resonances in each group, are of this type. Since Wannier (1953) was the first to realize the importance of the potential ridge region for determining the behaviour of low-energy two-electron systems, we refer to such resonances as '*Wannier-ridge*' resonances.

The He^- resonances can also be related to those that might arise from the Kellman–Herrick model described in Section 3. The lowest of the intrashell states having $n_1 = n_2 = n$ is that for which the quantum numbers v, J and l in equation (18) are all zero, and we assume that the internal structure of this state (giving rise to the internal energy term in equation 18) is that of a 'Wannier-ridge' state. The higher energy states of the supermultiplets presumably correspond to systems in which there is motion away from and through the Wannier ridge, in addition to motion along the ridge. An aspect of the rotational–vibrational model which is directly relevant to our present observations is that the predicted total span of energy ΔE_n of all the members of the supermultiplet corresponding to $n_1 = n_2 = n$ is equal to $2(n-1)\omega$, and that Herrick *et al.* (1980) find that ω is approximately proportional to $n^{-3.38}$ for He** and $n^{-3.25}$ for H^{-}**, causing ΔE_n to be approximately proportional to $(n-1)n^{-3.3}$ for both these atoms. At high values of n we see therefore that ΔE_n decreases with n more slowly (i.e. $n^{-2.3}$) than the energy spacing between the lowest levels of neighbouring multiplets (since this spacing is approximately proportional to n^{-3}, regardless of whether equation 13 or 31 is applicable). In other words the supermultiplets will begin to overlap at some sufficiently high value of n. As pointed

out above, we can see from Fig. 10 that this does indeed happen for the He^- resonances that we have observed.

Two additional points for which we can offer no explanation at present concern the heights and widths of the observed resonances. The ratios of the peak-to-valley heights of the lowest member of each supermultiplet to the mean yield at the corresponding resonance energy are given in Table 4. These ratios are approximately proportional to n^{-6}, but it must be remembered that the ratios are affected to an unknown extent when the resonances have natural widths less than the apparatus energy resolution, as seems to be the case for the higher lying resonances. As far as the widths themselves are concerned, these do not change smoothly with n. In particular, the lowest $n = 4$ resonance is noticeably broader than the lowest $n = 3$ and 5 resonances.

Table 5. Application of modified Rydberg formulae (13), (16) and (17) to configurations [core]ns^2 where n is higher than its lowest possible value

Values given in parentheses indicate error in last significant figure

Atom	Configuration	Parameter					Δ (%) using	
		Z_{core}	E (eV)	E_I (eV)	δ_{ns}	σ^A	eqn (16)	eqn (17)
H^-	$2s^2$	1	9·557	14·355	0	0·274	−5·38	−5·37
He	$2s^2$	2	57·82	79·005	0	0·235	−1·67	−2·81
He^-	$1s3s^2$	1	22·450(5)	24·588	0·265	0·233(1)	−4·3(2)	−2·9(2)
	$1s4s^2$	1	23·443(5)	24·588	0·262	0·233(2)	−4·3(4)	−1·9(4)
	$1s5s^2$	1	23·851(10)	24·588	0·260	0·220(5)	−7·6(13)	−4·7(13)
	$1s6s^2$	1	24·079(10)	24·588	0·260	0·215(8)	−8·7(18)	−5·5(18)
	$1s7s^2$	1	24·216(10)	24·588	0·259	0·212(11)	−9·5(25)	−6·0(25)

[A] From equation (13).

A further point of interest in the spectrum of Fig. 10 is the presence of the cusp-like feature at the ionization energy E_I (24·588 eV). The feature appears in this form after a sloping background has been subtracted from the measured yield. We see that the metastable excitation cross section rises as the incident energy approaches E_I, at which point a discontinuous decrease in slope occurs. The analogous features in the metastable excitation functions of argon and krypton have been observed previously by Brunt *et al.* (1976). Since the high-n Rydberg states of all these atoms are metastable they contribute to the observed yield in this region, but in all three cases this contribution is small and it consists of a sharp increase in the yield starting just below E_I (Hammond *et al.* 1982*a*), similar to that shown in Fig. 3 for H_2. Only in the case of xenon is this contribution significant, due to the very low detection efficiency for the lowest metastable states of this atom (Brunt *et al.* 1976). The cusp in Fig. 10 must therefore be present in the cross section of the 2^3S and 2^1S states and of other low-n states that cascade to these. Possible explanations of the existence of the cusp are (*a*) that it represents an accumulation of Wigner cusps due to the successive openings of the high-n excitation channels; (*b*) that it represents a Wigner cusp due to the opening of the ionization channel; (*c*) that it is caused by the series of high-n Wannier-ridge resonances that converge at E_I; or (*d*) that it is some other manifestation of the correlations that exist between two slow electrons.

(*c*) *Energy Parametrization*

Substitution of the Wannier-point potential energy (14) into Schrödinger's equation immediately gives the modified energy formula (13) with $\sigma = 0{\cdot}25$ and $\delta_{ns} = 0$, where n can have any value from its minimum to infinity (see also Heddle 1976, 1977). The results of applying the modified Rydberg formulae (13) and (16) and the extended form (17) to the measured energies of the Wannier-ridge resonances are given in Table 5. Also included are data for two other states of the type [core]ns^2, where n is higher than its minimum value. Clearly these three formulae are not as successful here as they are for the states of lowest n. The errors in using the semi-empirical formula (17) are however still small in absolute terms; for the H^- $2s^2$, He $2s^2$ and He^- $1s\,7s^2$ states, for example, the errors are $0{\cdot}25$, $0{\cdot}59$ and $0{\cdot}02$ eV respectively.

Using equation (28) to estimate the energy differences $2B$ between the $1s(ns\,np\ ^3P)^2P$ and the $1s(ns^2)^2S$ states, we find

$$2B(n) \approx 2{\cdot}4/(n-0{\cdot}26)^3 \text{ eV}, \tag{34}$$

which tends to be somewhat smaller (by a factor of ≈ 2) than the observed differences.

5. Conclusions

The theme that is common to the topics discussed in Sections 2, 3 and 4 is the importance of the Wannier-ridge region in determining the behaviour of systems that contain two slow electrons. These electrons may either both be unbound, as in the threshold ionization process, or one may be bound and the other free, as in the threshold excitation process, or both may be bound, as in negative-ion resonances. In all examples considered, the sum of the moduli of the total energies of the two electrons is small:

$$E_{\text{tot}} = |E_{\text{tot},1}| + |E_{\text{tot},2}| \lesssim 0{\cdot}5 \text{ eV}. \tag{35}$$

A theoretical connection between the three types of system has yet to be forged. The threshold ionization process has been adequately explained, but threshold excitation has been treated only qualitatively so far, as have the Wannier-ridge resonances. Clearly the time is ripe for a further theoretical advance.

Acknowledgments

The author is grateful to his colleagues Drs S. J. Buckman, P. Hammond, S. Cvejanović and G. C. King, for permission to include their recent results, and for their critical comments on the manuscript. He is also grateful to various other authors for permission to reproduce their figures.

References

Andrick, D. (1979). *J. Phys.* B **12**, L175.
Brunt, J. N. H., King, G. C., and Read, F. H. (1976). *J. Phys.* B **9**, 2195.
Brunt, J. N. H., King, G. C., and Read, F. H. (1977*a*). *J. Phys.* B **10**, 433.
Brunt, J. N. H., Read, F. H., and King, G. C. (1977*b*). *J. Phys.* E **10**, 134.
Bryant, H. C., *et al.* (1981). *In* 'Atomic Physics', Vol. 7 (Eds D. Kleppner and F. M. Pipkin), pp. 29–63 (Plenum: New York).
Buckman, S. J., Hammond, P., Clark, C. W., Taylor, K. T., King, G. C., and Read, F. H. (1982*a*). *J. Phys.* B (to be submitted).
Buckman, S. J., Hammond, P., King, G. C., and Read, F. H. (1982*b*). *J. Phys.* B (to be submitted).

Buckman, S. J., Hammond, P., King, G. C., and Read, F. H. (1982*c*). *J. Phys.* B (in press).
Burke, P. G., and McVicar, D. D. (1965). *Proc. Phys. Soc. London* **86**, 989.
Cooper, J. W., Fano, U., and Prats, F. (1963). *Phys. Rev. Lett.* **10**, 518.
Cowan, R. D. (1981). 'The Theory of Atomic Structure and Spectra' (Univ. California Press: Berkeley).
Cvejanović, S., and Read, F. H. (1974). *J. Phys.* B **7**, 1841.
Cvejanović, S., Hammond, P., King, G. C., and Read, F. H. (1982). *J. Phys.* B (to be submitted).
Fano, U., and Cooper, J. W. (1968). *Rev. Mod. Phys.* **40**, 44.
Fano, U. (1974). *J. Phys.* B **7**, L401.
Fano, U. (1976). Phys. Today **29** (No. 9), 32.
Fano, U. (1980). *J. Phys.* B **13**, L519.
Fano, U., and Lin, C. D. (1975). *In* 'Atomic Physics', Vol. 4 (Eds G. zu Putlitz, E. W. Weber and A. Winnacker), pp. 47–70 (Plenum: New York and London).
Greene, C. H. (1981). *Phys. Rev.* A **23**, 661.
Greene, C. H., and Rau, A. R. P. (1982). *Phys. Rev. Lett.* **48**, 533.
Hammond, P., King, G. C., and Read, F. H. (1982*a*). *J. Phys.* B (to be submitted).
Hammond, P., King, G. C., Read, F. H., and Warner, C. (1982*b*). *J. Phys.* B (to be submitted).
Heddle, D. W. O. (1976). *Contemp. Phys.* **17**, 443.
Heddle, D. W. O. (1977). *Proc. R. Soc. London* A **352**, 441.
Heideman, H. G. M., Van der Water, W., and Van Moergestel, L. J. M. (1980). *J. Phys.* B **13**, 2801.
Herrick, D. R., and Kellman, M. E. (1980). *Phys. Rev.* A **21**, 481.
Herrick, D. R., Kellman, M. E., and Poliak, R. D. (1980). *Phys. Rev.* A **22**, 1517.
Herrick, D. R., and Sinanoglu, O. (1975). *Phys. Rev.* A **11**, 97.
Iachello, F., and Rau, A. R. P. (1981). *Phys. Rev. Lett.* **47**, 501.
Kellman, M. E., and Herrick, D. R. (1978). *J. Phys.* B **11**, L755.
Kellman, M. E., and Herrick, D. R. (1980). *Phys. Rev.* A **22**, 1536.
Klar, H., and Klar, M. (1980). *J. Phys.* B **13**, 1057.
Klar, H., and Schlecht, W. (1976). *J. Phys.* B **9**, 1699.
Langlois, J., and Sichel, J. M. (1980). *J. Phys.* B **13**, 881.
Lin, C. D. (1974). *Phys. Rev.* A **10**, 1986.
Lin, C. D. (1975). *Phys. Rev. Lett.* **35**, 1150.
Lin, C. D. (1982). *Phys. Rev.* A **25**, 76.
Lipsky, L., Anania, R., and Connealy, M. J. (1977). At. Data Nucl. Data Tables **20**, 127.
Macek, J. (1968). *J. Phys.* B **1**, 831.
Madden, R. P., and Codling, K. (1963). *Phys. Rev. Lett.* **10**, 516.
Marchand, P., Paquet, C., and Marmet, P. (1969). *Phys. Rev.* **180**, 123.
Nesbet, R. K. (1978). *J. Phys.* B **11**, L21.
Peterkop, R. (1971). *J. Phys.* B **4**, 513.
Peterkop, R., and Liepinsh, A. (1981). *J. Phys.* B **14**, 4125.
Pichou, F., Huetz, A., Joyez, G., and Landau, M. (1978). *J. Phys.* B **11**, 3683.
Rau, A. R. P. (1971). *Phys. Rev.* A **4**, 207.
Read, F. H. (1977). *J. Phys.* B **10**, 449.
Read, F. H., Brunt, J. N. H., and King, G. C. (1976). *J. Phys.* B **9**, 2209.
Rehmus, P., Kellman, M. E., and Berry, R. S. (1978). *Chem. Phys.* **31**, 239.
Schulz, G. J. (1973). *Rev. Mod. Phys.* **45**, 378.
Simpson, J. A., and Fano, U. (1963). *Phys. Rev. Lett.* **11**, 158.
Spence, D. (1975). *Phys. Rev.* A **11**, 1539.
Tarr, S. M., Schiavone, J. A., and Freund, R. S. (1980). *Phys. Rev. Lett.* **44**, 1660.
Vinkalns, I., and Gailitis, M. (1967). *In* 'Fifth Int. Conf. on Physics of Electronic and Atomic Collisions' (Eds I. P. Flaks and E. S. Solovyov), pp. 648–50 (Nauka: Leningrad).
Wannier, G. H. (1953). *Phys. Rev.* **90**, 817.
Watanabe, S. (1982). *Phys. Rev.* A (in press).
Wulfman, C. (1973). *Chem. Phys. Lett.* **23**, 370.
Yuh, H.-J., Ezra, G., Rehmus, P., and Berry, R. S. (1981). *Phys. Rev. Lett.* **47**, 497.

Manuscript received 9 August, accepted 20 August 1982